

Organised motions in turbulent boundary layers over a wide range of Reynolds number

Kapil A. Chauhan^{*}, Ivan Marusic[†] and Nicholas Hutchins[‡]

Department of Mechanical Engineering, The University of Melbourne, Parkville, VIC 3010, Australia

The motivation behind this paper comes from the large-scale coherence that has been recently reported in the near-wall and logarithmic regions of wall-bounded turbulent flows. Associated with these are inclined vortical structures that populate the near-wall region. Most often these inclined structures have been inferred as hairpin shaped vortices that have been observed experimentally and evidenced using conditional averaging and two-point correlations. The objective of this study is to analyse three-component velocity fields and determine the instantaneous three-dimensional structure around these large-scale coherent motions and their concurrent existence in the laboratory and the neutral atmospheric surface layer. Starting from two-point correlation we further extend the interrogation of these structures via the instantaneous flow field. The instantaneous spanwise velocity field clearly shows the presence of vortical features that resemble the hairpin vortices. Results for spectra for the spanwise velocity component show that energy of large scales ($\sim 6\delta$) increases with increasing Reynolds number just like the streamwise component.

I. Introduction

Very long meandering structures of low-momentum streamwise fluid have been observed experimentally [e.g., Kim and Adrian, 1999, del Álamo et al., 2004, Guala et al., 2006, Hutchins and Marusic, 2007a, Monty et al., 2007, Bailey and Smits, 2010, and others] in the logarithmic and outer region ($z^+ > 100$, z is the wall-normal distance, and the $+$ superscript implies normalisation with the wall variables, U_τ and ν) of laboratory wall-bounded flows. These long structures also termed as ‘Superstructures’ [Hutchins and Marusic, 2007a] or Very Large Scale Motions [VLSMs, Kim and Adrian, 1999] are found in all three canonical wall-bounded flows; i.e., pipes, channels and boundary layers with slightly differing physical characteristics. Superstructures have been observed with lengths as large as 20δ (δ is the boundary layer thickness) in the streamwise direction and significantly contribute to the total turbulent stress. Further, it is observed that such features in the flow leave a statistical footprint in the two-point correlation [Hutchins and Marusic, 2007a, Marusic and Hutchins, 2008] and instantaneous skin-friction [Hutchins et al., 2011b]. As the superstructures seem to scale with outer variables their presence in the surface layer would imply that they occur at very large physical scales [$\mathcal{O}(100\text{m})$]. Similar observations regarding long regions of low- and high-speed regions in the atmospheric surface layer (ASL) are made in large-eddy simulation (LES) by Moeng and Sullivan [1994] and Lin et al. [1997], although the relationship between these features and the superstructures observed in laboratory flows is as yet unclear.

It is also suggested that superstructures are caused by pseudo-streamwise alignment of large-scale motions (LSMs) which are identified by low-speed streamwise fluid that is trapped between packets of hairpin vortices moving at the same convection velocity [Kim and Adrian, 1999, Adrian, 2007]. Hairpin vortices have been extensively studied in laboratory flows [Head and Bandyopadhyay, 1981, Christensen and Adrian, 2001, Adrian et al., 2000, Ganapathisubramani et al., 2003, 2005, Wu and Christensen, 2006, Dennis and Nickels, 2011, and others] and numerical investigations [Zhou et al., 1999, Wu and Moin, 2009, Lee and Sung, 2011]. Hairpins are believed to be organised in a ramp-like structure and can extend up to the outer edge of the boundary layer. Flow visualisation by Hommema and Adrian [2003] and particle image velocimetry

^{*}Research Fellow, and AIAA member. kchauhan@unimelb.edu.au

[†]Professor, and AIAA member

[‡]Lecturer

(PIV) by Morris et al. [2007] in the atmospheric surface layer has been unable to document the presence of hairpins with the same clarity as has been found in laboratory flows. However, ramp-like shear layers which are typical signatures of hairpin vortex packets were observed. Phong-Anant et al. [1980] obtained temperature traces at several heights in the first 8 m of the atmospheric surface layer that indicated the presence of a ramp-like interface in the temperature profile, the inclination of which increased with height. Vortical structures with a horseshoe-like form were found in LES of neutrally stratified planetary boundary layer (PBL) by Lin et al. [1996], but of quite a different scale than those in a flat plate turbulent boundary layer. Many other experimental efforts have also focussed on identifying the three-dimensional structure of the surface layer [Högström and Bergström, 1996, Carper and Porté-Agel, 2004, Marusic and Heuer, 2007, Guala et al., 2010]. In the neutral surface layer, Carper and Porté-Agel [2004] found vortical structures in the downstream direction at angles of about 16° . Using linear stochastic estimates (LSE), Hutchins and Marusic [2007b] showed that a large-scale counter-rotating structure is present near the long low-speed region in an averaged flow field.

	U_∞	u_τ	δ	Re_τ
Laboratory BL	6 m/s	0.25 m/s	0.068 m	1100
Neutral ASL	$U(z=2.14\text{m})=5.56$ m/s	0.1825 m/s	≈ 60 m	$\approx 6.3 \times 10^5$

Table 1. Flow characteristics.

II. Experimental details

Two experimental measurements are specifically examined for the spanwise velocity component. The first set of data consists of stereoscopic particle image velocimetry measurements taken in a zero pressure gradient turbulent boundary layer by Hambleton et al. [2006]. The second set of data is from atmospheric surface layer (ASL) measurements under neutral conditions acquired using an array of 18 sonic anemometers by Hutchins et al. [2011a]. The flow parameters for the two experiments are listed in table 1. These two experiments are unique as they have simultaneous measurements in the streamwise/wall-normal (x - z) and streamwise-spanwise (x - y) planes, while their Reynolds number differ by three orders of magnitude. Here x , y , and z refer to the streamwise, spanwise and wall-normal directions, respectively. For the laboratory data, the PIV in the horizontal plane is located at $z/\delta = 0.088$ and spans 1.65δ and 2δ in the x and y directions, respectively. The PIV in the vertical plane measures from $z/\delta = 0.02$ to $z/\delta = 1.53$ and 1.65δ in the x direction. In the surface layer measurements 10 sonic anemometers are placed equidistant spanning a width of 27 m at a height of $z/\delta = 0.036$. Additional 8 sonics are placed logarithmically from $z/\delta = 0.019$ extending up to a total height of $z/\delta = 0.43$ to form an ‘L’ shaped array. The neutral surface layer is considered to be appropriate for comparison with the zero pressure gradient laboratory data based on the similarity of its mean and correlation statistics concluded by Marusic and Hutchins [2008] and Hutchins et al. [2011a]. The reader is referred to Marusic and Hutchins [2008] and Hambleton et al. [2006] for further details about the experimental setup and processing. All three components of velocity are measured in the two experiments making them suitable for event based analysis of flow features and instantaneous three-dimensional characteristics.

III. Results

A. Two-point correlations

With the unique measurement setup in both the experiments under consideration, a reference or condition point can be chosen that is common to both the spanwise and the wall-normal plane. In the PIV, this point is chosen as a position along the line of intersection of the horizontal and vertical PIV planes, while for the ASL measurements the sonic anemometer that is common to the spanwise and wall-normal array is the reference point. Using the condition point one can now get a ‘combined’ two-point correlation map. Moreover if the condition point is relocated to a position in the spanwise plane that is away from the wall-normal plane one is able to investigate the two-point correlation coefficient over an altered spatial domain. Such an approach gives multiple combined spanwise/wall-normal two-point correlation maps that fill up a pseudo-volume. A

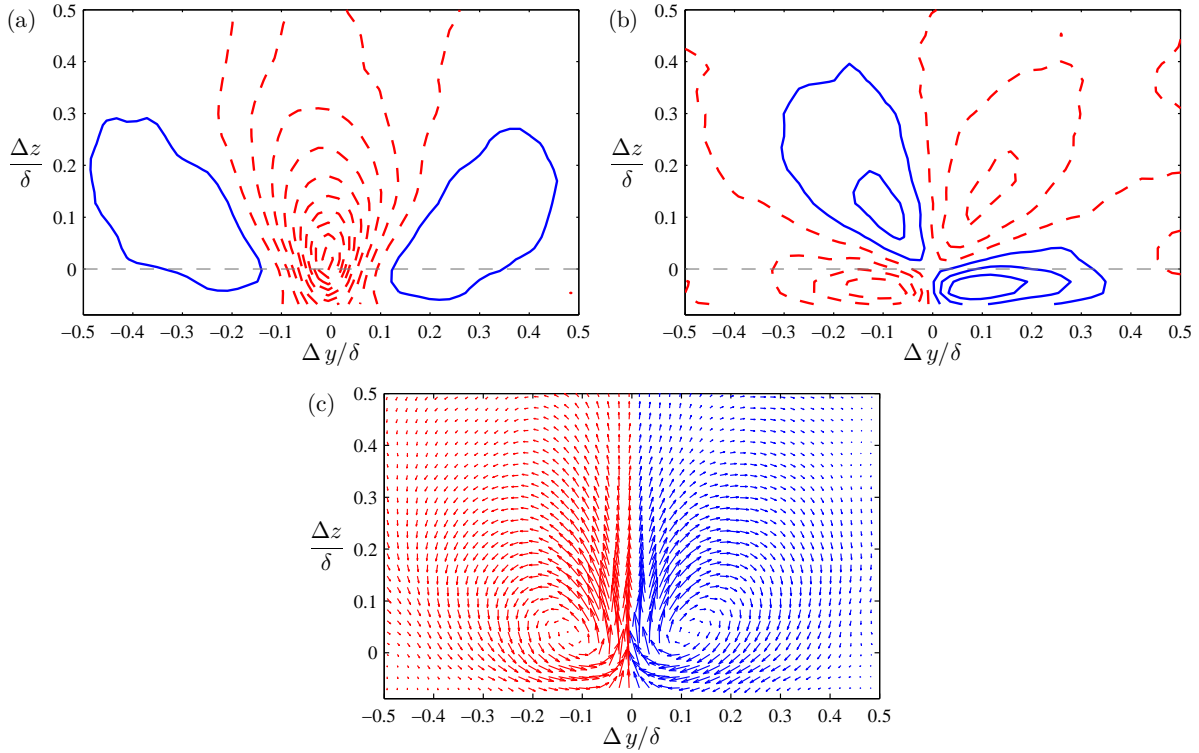


Figure 1. (a) Two-point correlation, R_{uw} in the spanwise - wall-normal (y - z) plane. (b) Two-point correlation, R_{uv} in the spanwise - wall-normal (y - z) plane. (b) Two-point correlation, R_{uv} in the spanwise - wall-normal (y - z) plane. All three plots are for the laboratory boundary layer. For (a) and (b), contour levels are in increments of ± 0.05 , negative contour levels are shown in dashed red lines, positive contour levels are in solid red and dashed gray line indicates location of horizontal PIV plane ($z/\delta \approx 0.088$) considered as reference. (c) Linear stochastic estimate based on a negative u event at the condition point $\Delta y = 0$, $z/\delta \approx 0.088$.

volumetric correlation map is thereby obtained. This process has been previously illustrated by Marusic and Hutchins [2008] and Hutchins et al. [2011b] in laboratory measurements to map volumetric correlation information from simultaneously sampled orthogonal arrays / PIV planes.

Figure 1(a) shows the two-point cross-correlation map of R_{uw} in the spanwise/wall-normal plane obtained from the PIV in horizontal and vertical planes. It is found that a large region of negative correlation exists near $\Delta y = 0$ from the wall to the outer part of the boundary layer. The negative R_{uw} implies that in this region u and w most likely have opposite signs as one would expect for Q2 ($u < 0$, $w > 0$) and Q4 ($u > 0$, $w < 0$) events. The negative R_{uw} is symmetrically flanked by positive R_{uw} on either side, clearly demarcated by the zero level contour line. Hence, when a negative u event occurs near $\Delta y = 0$ a positive w fluctuation is most likely to be encountered around it, while a negative w fluctuation is more likely to flank it on either side (at $\Delta y \approx \pm 0.3\delta$). The same can be said for a positive u event leading to w fluctuations taking opposite signs. Similarly, figure 1(b) shows the two-point cross-correlation map of R_{uv} in the spanwise-wall-normal plane. Here it is seen that four distinct regions of positive and negative R_{uv} are present. The cross-correlation R_{uv} has opposite sign on either side of $\Delta y = 0$, however it also changes signs further away from the wall in z . If a negative u event occurs near $\Delta y = 0$, the R_{uv} map suggests that the spanwise velocity will be converging near the wall at $\Delta y = 0$, while in the outer region they will be diverging.

We can use these correlation maps to produce a Linear Stochastic Estimate (LSE) based on the occurrence of negative u fluctuations (a low-speed event) at the condition point $\Delta y = 0$, $z/\delta \approx 0.088$ in the laboratory data [see Adrian and Moin, 1988, Tomkins and Adrian, 2003, for a description of this technique]. For this simple detection event, the linear stochastic estimate) is merely a function of the two-point cross correlations R_{uu} , R_{uv} and R_{uw} calculated on unconditional data [Hutchins et al., 2005]. Using the LSE on R_{uw} and R_{uv} for a conditional low-speed u event occurring at $\Delta y = 0$ and $z/\delta = 0.088$, a conditional (v , w) vector field in the $y - z$ cross-plane is obtained and shown in figure 1(c). It is readily observed that the linear stochastic estimate results in a counter-rotating roll-mode that ejects the near wall fluid away from the wall

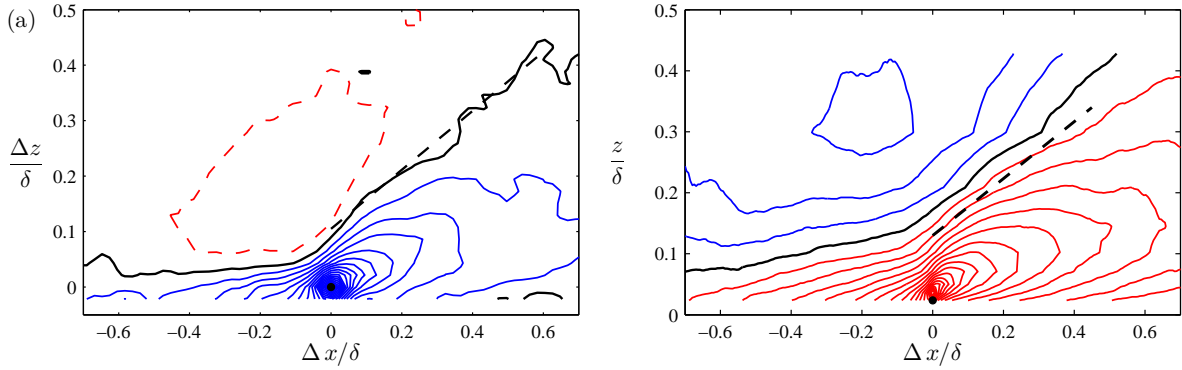


Figure 2. Two-point correlation, R_{vv} in the streamwise-wall-normal (x - z) plane. (a) Laboratory boundary layer at $Re_\tau = 1100$. The reference point is located $\Delta x = 0$, $z/\delta = 0.042$ (b) Neutral atmospheric surface layer data at $Re_\tau \approx \mathcal{O}(10^6)$. The reference point is located $\Delta x = 0$, $z/\delta = 0.036$. Zero contour level is shown in black, positive contour levels are shown in solid blue line, negative contour levels are shown in dashed red lines, and contour levels are in increments of ± 0.05 .

at $\Delta y = 0$. Similar large scale roll-modes have been observed by Hutchins and Marusic [2007b], Marusic and Hutchins [2008], Chung and McKeon [2010]. Lin et al. [1996] and Foster et al. [2006] in their LES study also found counter-rotating roll-modes near the wall associated with conditionally sampled sweep events and ejection events, respectively. Figure 1 reinforces the notion of counter-rotating roll-modes occurring between elongated high and low u momentum regions. The counter rotating rolls would have an opposite sense of rotation if the LSE event is conditioned for a high-speed u event. Such a schematic of low-speed fluid between two counter-rotating rolls fits well with the hair-pin packets paradigm, where the legs of the multiple hairpins orient themselves around low momentum streamwise flow. Based on figure 1(c) two characteristics are identified that appear to occur simultaneously in the flow over a superstructure. They are: (1) Spanwise convergence - by the v fluctuations towards each other near the wall (away from each other at higher z/δ), and (2) Upwash - ejection of fluid away from the wall by positive w fluctuations. It should be noted that the large roll-modes explained here are very different from the quasi-two-dimensional structures that occur in the convective mixed layer and are also called rolls [LeMone, 1973, Khanna and Brasseur, 1998, Young et al., 2002]. Such convective rolls are basically buoyancy induced motions that form alternating regions of updrafts ($+w$) and downdrafts ($-w$). These motions extend throughout the atmospheric boundary layer depth and are much bigger in size than the shear induced roll-modes discussed above. It should also be reiterated that these modes are completely different from the near-wall cycle of streaks and quasi-streamwise vortices, which in the ASL will be three orders of magnitude smaller.

It is deduced from LSE that roll-modes occurring near low- or high-momentum streamwise fluid will induce positive and negative spanwise velocity as one moves away from the wall. We will therefore, for this study, examine the spanwise velocity component (this component has typically been overlooked in previous studies of streamwise/wall-normal planes). Figures 2(a) and 2(b) show the two-point correlation map of R_{vv} in the streamwise-wall-normal plane for the laboratory boundary layer and the neutral surface layer, respectively. The reference location for the laboratory flow is at $z/\delta = 0.042$, while for the surface layer it is at $z/\delta \approx 0.036$. The streamwise ordinate for the ASL data is recovered using the Taylor's hypothesis and a mean convection velocity $U_c = 5.57 \text{ m s}^{-1}$ obtained from the spanwise array. One can see remarkable similarity in the overall characteristics of the R_{vv} map in both these flows despite their Re_τ being different by three orders of magnitude. Near the condition point (shown by the solid symbol close to the wall), long regions of positive correlation exist, while in the outer part of the boundary layer it is predominantly negative. The zero level contour line is emphasised in these plots to distinguish the positive and negative regions. The zero line also shows different orientation upstream and downstream of the reference point. Upstream of $\Delta x = 0$ it appears to be linear with a very shallow angle relative to the surface. This angle increases steeply downstream of $\Delta x = 0$, but the linearity remains intact. For the laboratory data, this angle is found to be 25° while it is 28° for the ASL and is indicated by a dashed line in the plots. The zero R_{vv} correlation line could be considered as the footprint of longitudinal rolls or vortical motions whose core lies on the zero line (and hence have a zero v component) with oppositely signed v above and below. This characteristic

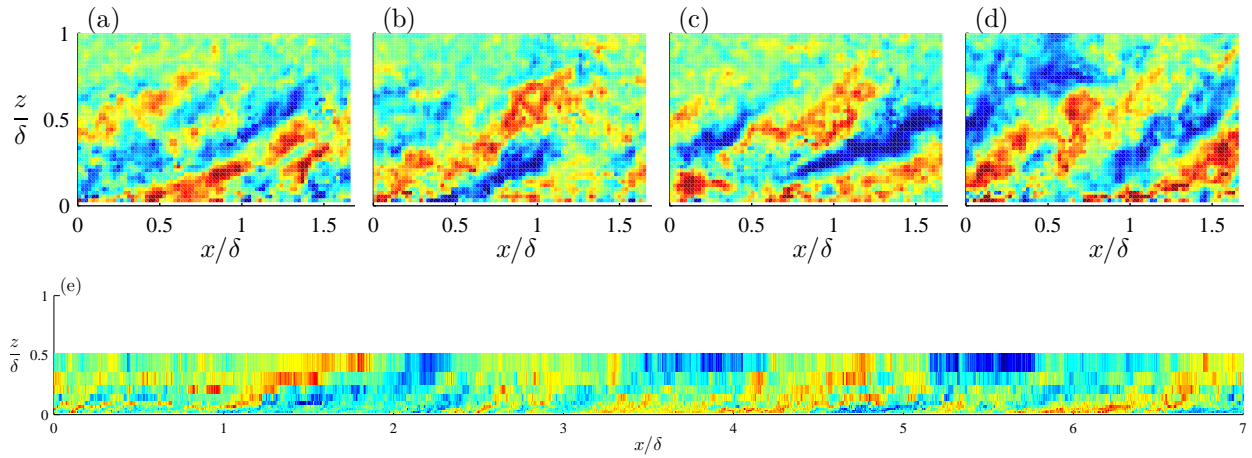


Figure 3. Instantaneous spanwise velocity fluctuations in the streamwise-wall-normal (x - z) plane. High positive v regions are indicated by red while blue denotes highly negative v regions. (a - d) are instantaneous PIV snapshots from laboratory boundary layer, $Re_\tau = 1100$.(e) Neutral ASL data projected using Taylor's hypothesis, $Re_\tau \approx \mathcal{O}(10^6)$. It should be noted that the PIV data in (a-d) is not sequential.

agrees with the presence of roll modes in the LSE vector field of figure 1(c). Further, the shape of the zero line with two distinct angles but linear orientation before and after $\Delta x = 0$ is also similar to the shape of hairpin vortices proposed in the literature. Typical inferred hairpin vortex structures have been proposed with inclination angles that are much steeper at the head than at the legs (see example given later in figure 5). This is entirely consistent with the two-point correlations of figure 2. The inclination angle of 25° away from the wall is small compared to original findings of Head and Bandyopadhyay [1981] (about 45°) but in very good agreement with 26.5° found by Dennis and Nickels [2011]. In the laboratory hairpin vortices have been well-documented (e.g. [Adrian et al., 2000, Christensen and Adrian, 2001, Ganapathisubramani et al., 2003, 2005, Lee and Sung, 2011, etc.]), while in the ASL they have been inferred but not conclusively found [Hommema and Adrian, 2003, Morris et al., 2007]. Past studies involving PIV have focussed largely on detecting swirl events or vortex cores as signature of hairpin vortices in the streamwise/wall-normal plane or the spanwise/wall-normal plane. Here we have chosen to examine the induced velocity field, specifically the spanwise velocity component in the wall-normal plane which would be significant in the leg or arch of a typical hairpin structure. It appears that the inclined feature, typical of hairpin-like vortices, is present in the surface layer too and extend up to at least 0.5δ (30 m) in the wall-normal direction. The instantaneous spanwise velocity field shown in figure 3 provides further evidence of this.

B. Instantaneous structure

It is important to examine if the spanwise flow field suggested by the two-point R_{vv} correlation map does actually occur in the boundary layer. With this objective we look at the instantaneous spanwise velocity field in the streamwise-wall-normal plane for the laboratory and the surface layer flows in figure 3(a-e). The instantaneous spanwise velocity in figure 3 is normalised by the corresponding v_{rms} . For the surface layer data the spatial flow field up to 7δ in x is projected using Taylor's hypothesis, while the PIV flow field was limited to 1.7δ in x due to the limited viewing range of the cameras. Nonetheless, four representative PIV planes are shown here to approximate the 7δ view shown for the ASL with equivalent scale. In figures 3(a-d) the spanwise velocity shows 'stripiness'; i.e., alternating inclined regions of positive and negative fluctuations. These stripes of bulk positive or negative v stretch all the way from the wall to the core of the boundary layer. Multiple instances are shown to emphasise that such features are abundantly present in the flow^a. The positive/negative coupling of the spanwise fluctuations with similar physical orientation may suggest the presence of similar inclined vortical motions in both flows. Similar very distinct alternating stripes of positive/negative v are also observed in the neutral surface layer. The wall-normal extent of the flow field here is limited by the maximum height of the sonic anemometer array. Nevertheless we see these alternating

^aPIV data in plots (a-d) are not sequential

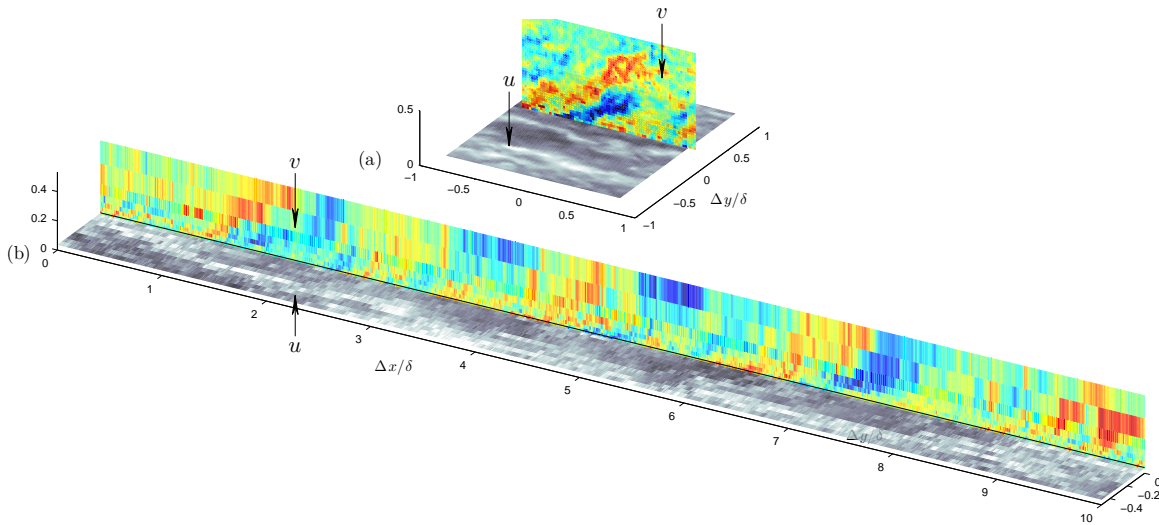


Figure 4. Instantaneous spanwise velocity fluctuations in the streamwise-wall-normal (x - z) plane and instantaneous streamwise velocity fluctuations in the streamwise/spanwise (x - y) plane. High positive v regions are indicated by red while blue denotes highly negative v regions. High negative u regions are indicated by dark gray while light gray shade denotes highly positive u regions. (a) Instantaneous PIV snapshots from laboratory boundary layer, $Re_\tau = 1100$. (e) Neutral ASL data projected using Taylor's hypothesis, $Re_\tau \approx \mathcal{O}(10^6)$.

inclined spanwise motions extending at least up to 0.5δ . In the ASL these vortical motions have a large physical extent, $\mathcal{O}(10\text{m})$ compared to the laboratory flow where they are $\mathcal{O}(0.01\text{m})$, signifying the wide range of scales over which the underlying mechanisms can exist in a flow. These extend at least up to 30m in the surface layer measurements and the inclination angle appears to be shallow near the wall for uniform spanwise velocity regions. Consistent with the similarity of R_{vv} between the laboratory and atmospheric flow observed in figure 2, we find that the instantaneous velocity fields also have a strong resemblance. For both flows the instantaneous v velocity field agrees with the spanwise velocity induced by the counter-rotating rolls suggested by the LSE in figure 1 and/or inclined vortices inferred from R_{vv} in figure 2. It would be premature to attribute each of the striped regions observed in the neutral surface layer to a single hair-pin vortex moving with the flow in the neutral surface layer. This is because the acquisition by sonic anemometers with logarithmic spacing inherently has low spatial resolution and the projected instantaneous field is high-pass filtered due to low sampling rates.

The same instantaneous spanwise velocity field in the wall-normal plane of figures 3(b) and 3(e) is also shown in figure 4 along with the streamwise velocity fluctuations in the spanwise plane. In the spanwise plane the streamwise velocity fluctuations show distinct regions of long uniform momentum regions appearing as alternating stripes of positive and negative u fluctuations. This is only observed over an extent of about 1.7δ in the PIV results. For the ASL a very distinct long meandering low-speed region is observed in the spanwise plane. This superstructure is at least 6δ long with high speed regions on either side. For both the laboratory and the ASL data, it is noted that there are distinctive inclined regions of alternating positive and negative spanwise velocity in the streamwise/wall-normal planes, when these planes are flanking the superstructure events. This observation is in support of the hairpin packet paradigm which proposes clusters of hairpin stacked together that convect in the flow residing over uniform streamwise momentum zones [Kim and Adrian, 1999, Adrian, 2007].

To qualitatively examine the occurrence of inclined spanwise velocity regions due to hairpin vortex packet, a synthetic flow field is created using a hairpin packet model in figure 5. Vortex lines in the shape of hairpins are stacked together aligned with the flow direction and the induced velocity field around these vortex lines is calculated using the Biot-Savart law. Contours of spanwise velocity in the streamwise/spanwise and streamwise/wall-normal planes are shown. The streamwise/wall-normal plane is chosen such that it cuts through the inclined legs in the hairpin packet. It is found that alternating regions of positive and negative spanwise velocity are formed in the wall-normal plane which characteristically look similar to the inclined

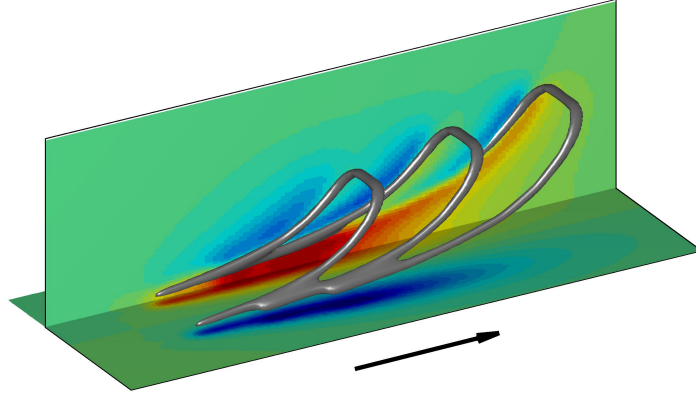


Figure 5. Spanwise velocity in the streamwise/wall-normal plane induced by a packet of hairpin vortices. The velocity field is calculated using the Biot-Savart law for vortex lines in the core of the hairpin shapes shown.

regions observed in figure 3. The figure also indicates that it is likely that the stripiness observed in the instantaneous field is due to a packet of vortices moving together instead of just a single hairpin vortex. Note that in a filtered view the packet would appear as a single inclined negative and positive spanwise velocity region in the streamwise wall-normal plane. Hence the spanwise velocity map very distinctly reveals the large scale characteristic of vortical structures but fails to clearly detect individual hairpin vortices from clusters or packets of vortices. The similarity in statistics and instantaneous features of spanwise fluctuations however confirm that hairpin-like vortices or packets are present over a wide range of physical scales [$\mathcal{O}(10^{-2}\text{m})$ - $\mathcal{O}(10\text{m})$] and Reynolds number [$\mathcal{O}(10^3)$ - $\mathcal{O}(10^6)$]. This observation is in contrast to the suggestion of Guala et al. [2010], that the hairpin model in surface layer flows may only be confined in the near-wall layer of $z^+ = \mathcal{O}(10^3)$, as in the present case the minimum $z^+ > 10^4$.

C. Spectra

In the previous section we showed that the spanwise fluctuations play a major role in the organisation of vortical motions around a superstructure. From the instantaneous field and two-point correlation map it is found that length scales associated with bulk regions of uniform spanwise fluctuations are of the order of boundary layer thickness. It is known from the statistics of streamwise fluctuations that the energy content of large scale motions increases with Reynolds number [Marusic et al., 2010]. Since the organised features in the spanwise velocity are observed to be closely associated with organised motions in the streamwise fluctuations (figure 4) it is useful to look at the energy content of the spanwise fluctuations too. Figure 6 shows the pre-multiplied spectra for all three components of velocity from two different measurements. Three component measurements at $Re_\tau = 7300$ by Hutchins et al. [2007] using x-wire in the high Reynolds number boundary layer wind tunnel (HRNBLWT) at the University of Melbourne are also shown for comparison with the spectra from neutral ASL. The wall-normal location at which the spectra is acquired is $z/\delta = 0.036$ for the hot-wire and ASL measurements. Our focus here is to examine the large-scale energy content and, as expected, the energy content of streamwise fluctuations increases with increasing Reynolds number near $\lambda_x \approx 6\delta$. Similarly the large-scale energy of the spanwise fluctuations is also noted to increase significantly near $\lambda_x \approx 6\delta$ with increasing Re_τ . Even at $Re_\tau = 7300$, it is observed that the spanwise fluctuations have substantial energy in the large-scales as compared to the wall-normal fluctuations. Hence the spectra provide support for large-scale interactions between u and v components in the form of superstructure events that are found to co-occur with the vortical features in the wall-normal plane as seen in the instantaneous flow field in figure 4. On the other hand the wall-normal fluctuations have a very weak large scale component over the wide range of Reynolds number presented due to the blocking effect from the wall.

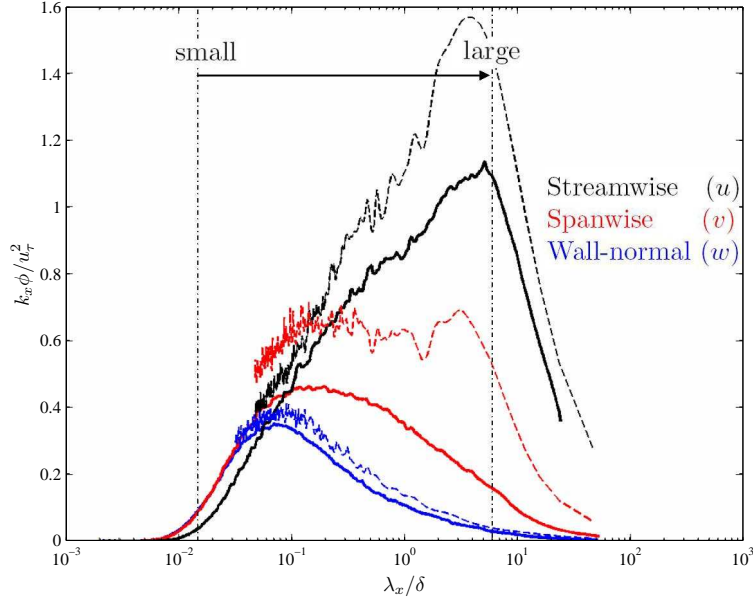


Figure 6. Pre-multiplied spectra $k_x \phi$ for three components of velocity. $k_x \phi_{uu}$, $k_x \phi_{vv}$ and $k_x \phi_{ww}$ are indicated by the colors black, red and blue respectively. Solid lines are from Hutchins et al. [2007] and dashed lines are for the ASL measurements.

IV. Conclusions

Two different turbulent boundary layer data-sets, each at opposite extremes of the Reynolds number range for physical flows have been compared for similarities in turbulence structure. The particular emphasis on the spanwise velocity provides a new perspective on vortical motions that are present in both laboratory and atmospheric surface layer flows. Simultaneous measurement of all three components of velocity in streamwise/spanwise and streamwise/wall-normal planes utilised in the two experiments is important for the analysis presented. The linear stochastic estimate helped us to reveal the conditional 3-D flow field around a superstructure near the wall in form of upwash and counter-rotating roll modes. Further the instantaneous spanwise velocity in the wall-normal plane attests to the notion of vortical features aligned with the flow direction. Two-point correlation R_{vv} draws an average picture of such vortical motion and exhibits remarkable similarity between laboratory and ASL flows. This implies that the inclined stripiness in the v field in these flows has the same underlying mechanism. However, characteristic shape of the R_{vv} map should be interpreted with caution as it allures one to the conclude that inclined stripiness is due to a hairpin vortex convecting past. The instantaneous flow field shows that the physical size of vortical features is large and well-organised. It is very unlikely for a single hairpin to independently exist and occupy more than 0.5δ of the layer thickness. Considering the hierarchical organisation of hairpin vortices in a hairpin packet that has been previously documented in laboratory flows and the small-scale filtering that is present in PIV and sonic anemometer measurements, it is more likely that the instantaneous v field shows the footprint of packets or clusters of vortices. Using Biot-Savart calculations on a packet of hairpin shaped vortex lines, it is found that a packet of hairpin vortices would result in distinctive regions of inclined $\pm v$ fluctuations in the streamwise/wall-normal plane. The instantaneous flow field also provides evidence of these vortical structures co-existing around the long meandering superstructure events. Such similarities in the instantaneous flow field between both studies suggest that the log region motions exhibit close dynamical similarity over a very large range of Reynolds number. The fully-mapped energy spectra in these flows support this conclusion. The large scale energy content of streamwise fluctuations increases with Reynolds number and with it the energy of spanwise fluctuations also grows. The significant increase in energy of u and v fluctuations at the large scales indicates that the superstructure and large-scale roll-modes are most likely inter-related.

Acknowledgments

This work was supported by funding from the Australian Research Council.

References

- R. J. Adrian. Hairpin vortex organization in wall turbulence. *Phys. Fluids*, 19(04):1301, 2007.
- R. J. Adrian and P. Moin. Stochastic estimation of organized turbulent structure: homogeneous shear flow. *J. Fluid Mech.*, 190:531–559, 1988.
- R. J. Adrian, C. D. Meinhart, and C. D. Tomkins. Vortex organization in the outer region of the turbulent boundary layer. *J. Fluid Mech.*, 422:1–54, 2000.
- S. C. C. Bailey and A. J. Smits. Experimental investigation of the structure of large- and very-large-scale motions in turbulent pipe flow. *J. Fluid Mech.*, 651:339–356, 2010.
- M. A. Carper and F. Porté-Agel. The role of coherent structures in subfilter-scale dissipation of turbulence measured in the atmospheric surface layer. *J. Turb.*, 5(40), 2004.
- K. T. Christensen and R. J. Adrian. Statistical evidence of hairpin vortex packets in wall turbulence. *J. Fluid Mech.*, 431:433–443, 2001.
- D. Chung and B. J. McKeon. Large-eddy simulation of large-scale structures in long channel flow. *J. Atmos. Sci.*, 661:341–364, 2010.
- J. C. del Álamo, J. Jiménez, P. Zandonade, and R. D. Moser. Scaling of the energy spectra of turbulent channels. *J. Fluid Mech.*, 500:135–144, 2004.
- D. J. C. Dennis and T. B. Nickels. Experimental measurement of large-scale three-dimensional structures in a turbulent boundary layer. Part 1. Vortex packets. *J. Fluid Mech.*, 673:180–217, 2011.
- R. C. Foster, F. Vianey, P. Drobinski, and P. Carlotti. Near-surface coherent structures and the vertical momentum flux in a large-eddy simulation of the neutrally-stratified boundary layer. *Boundary-Layer Meteor.*, 120(2):229–255, 2006.
- B. Ganapathisubramani, E. K. Longmire, and I. Marusic. Characteristics of vortex packets in turbulent boundary layers. *J. Fluid Mech.*, 478:35–46, 2003.
- B. Ganapathisubramani, N. Hutchins, W. T. Hambleton, E. K. Longmire, and I. Marusic. Investigation of large-scale coherence in a turbulent boundary layer using two-point correlations. *J. Fluid Mech.*, 524: 57–80, 2005.
- M. Guala, S. Hommema, and R. Adrian. Large-scale and very-large-scale motions in turbulent pipe flow. *J. Fluid Mech.*, 554:521–542, 2006.
- M. Guala, M. Metzger, and B. J. McKeon. Intermittency in the atmospheric surface layer: Unresolved or slowly varying? *Physica D*, 239:1251–1257, 2010.
- W. T. Hambleton, N. Hutchins, and I. Marusic. Simultaneous orthogonal-plane particle image velocimetry measurements in a turbulent boundary layer. *J. Fluid Mech.*, 560:53–64, 2006.
- M. R. Head and P. Bandyopadhyay. New aspects of turbulent boundary-layer structure. *J. Fluid Mech.*, 107:297–337, 1981.
- U. Högström and H. Bergström. Organized turbulence structures in the near-neutral atmospheric surface layer. *J. Atmos. Sci.*, 53(17):2452–2464, 1996.
- S. Hommema and R. J. Adrian. Packet structure of surface eddies in the atmospheric boundary layer. *Boundary-Layer Meteor.*, 106:147 – 170, 2003.

- N. Hutchins and I. Marusic. Evidence of very long meandering streamwise structures in the logarithmic region of turbulent boundary layers. *J. Fluid Mech.*, 579:1–28, 2007a.
- N. Hutchins and I. Marusic. Large-scale influences in near-wall turbulence. *Phil. Trans. Royal Soc. Lond. A*, 365:647–664, 2007b.
- N. Hutchins, W. T. Hambleton, and I. Marusic. Inclined cross-stream stereo particle image velocimetry measurements in turbulent boundary layers. *J. Fluid Mech.*, 541:21–54, 2005.
- N. Hutchins, I. Marusic, and M. Chong. Fully mapped energy spectra in a high Reynolds number turbulent boundary layer. In *Proc 11th EUROMECH European Turbulence Conference*, 2007.
- N. Hutchins, I. Marusic, K. Chauhan, J. Monty, and J. Klewicki. Towards reconciling the structure of boundary layers in the atmosphere and laboratory. *Boundary-Layer Meteorol.*, 2011a. In preparation.
- N. Hutchins, J. P. Monty, B. Ganapathisubramani, H. C. H. Ng, and I. Marusic. Three-dimensional conditional structure of a high-Reynolds-number turbulent boundary layer. *J. Fluid Mech.*, 673:255–285, 2011b.
- S. Khanna and J. Brasseur. Three-dimensional buoyancy- and shear-induced local structure of the atmospheric boundary layer. *J. Atmos. Sci.*, 55(5):710–743, 1998.
- K. C. Kim and R. Adrian. Very large-scale motion in the outer layer. *Phys. Fluids*, 11:417–422, 1999.
- J. H. Lee and H. J. Sung. Very-large-scale motions in a turbulent boundary layer. *J. Fluid Mech.*, 673:80–120, 2011.
- M. A. LeMone. The structure and dynamics of horizontal roll vortices in the planetary boundary layer. *J. Atmos. Sci.*, 30(6):1077–1091, 1973.
- C.-L. Lin, J. C. McWilliams, C.-H. Moeng, and P. P. Sullivan. Coherent structures and dynamics in a neutrally stratified planetary boundary layer flow. *Phys. Fluids*, 8(10):2626, 1996.
- C.-L. Lin, C.-H. Moeng, P. P. Sullivan, and J. C. McWilliams. The effect of surface roughness on flow structures in a neutrally stratified planetary boundary layer flow. *Phys. Fluids*, 9(11):3235, 1997.
- I. Marusic and W. Heuer. Reynolds number invariance of the structure inclination angle in wall turbulence. *Phys. Rev. Lett.*, 99(114504), 2007.
- I. Marusic and N. Hutchins. Study of the log-layer structure in wall turbulence over a very large range of Reynolds number. *Flow Turb. Combust.*, 81:115–130, 2008.
- I. Marusic, R. Mathis, and N. Hutchins. High Reynolds number effects in wall turbulence. *Int. J. Heat and Fluid Flow*, 31:418–428, 2010.
- C.-H. Moeng and P. P. Sullivan. A comparison of shear- and buoyancy driven planetary boundary layer flows. *J. Atmos. Sci.*, 51:999, 1994.
- J. Monty, J. Stewart, R. Williams, and M. Chong. Large-scale features in turbulent pipe and channel flows. *J. Fluid Mech.*, 589:147–156, 2007.
- S. C. Morris, S. R. Stolpa, P. E. Slaboch, and J. C. Klewicki. Near-surface particle image velocimetry measurements in a transitionally rough-wall atmospheric boundary layer. *J. Fluid Mech.*, 580:319–338, 2007.
- D. Phong-Anant, R. A. Antonia, A. J. Chambers, and S. Rajagopalan. Features of the organized motion in the atmospheric surface layer. *J. Geophys. Res.*, 85(C1):424–432, 1980.
- C. D. Tomkins and R. J. Adrian. Spanwise structure and scale growth in turbulent boundary layers. *J. Fluid Mech.*, 490:37–74, 2003.
- X. Wu and P. Moin. Direct numerical simulation of turbulence in a nominally zero-pressure-gradient flat-plate boundary layer. *J. Fluid Mech.*, 630:5–41, 2009.

- Y. Wu and K. T. Christensen. Population trends of spanwise vortices in wall turbulence. *J. Fluid Mech.*, 568:55–76, 2006.
- G. S. Young, D. A. R. Kristovich, M. R. Hjelmfelt, and R. C. Foster. Rolls, streets, waves, and more: A review of quasi-two-dimensional structures in the atmospheric boundary layer. *Bull. Amer. Meteorol. Soc.*, 83(7):997–1001, 2002.
- J. Zhou, R. J. Adrian, S. Balachandar, and T. M. Kendall. Mechanisms for generating coherent packets of hairpin vortices in channel flow. *J. Fluid Mech.*, 387:353–396, 1999.